DOI: 10.1002/ejic.201100326

Low-Temperature Hydrothermal Synthesis of Ultrafine Strontium Hexaferrite Nanoparticles

Darinka Primc,*[a] Miha Drofenik,[a,b] and Darko Makovec[a]

Keywords: Strontium / Iron / Nanoparticles / Hydrothermal synthesis / Magnetic properties

Ultrafine strontium hexaferrite ($SrFe_{12}O_{19}$) nanoparticles have been synthesized by the hydrothermal treatment of an appropriate suspension of Sr and Fe hydroxides in the presence of a large excess of OH^- at temperatures between 130 and 170 °C. To avoid the parallel formation of any undesired hematite (α-Fe_2O_3) during the synthesis, a large excess of Sr in the starting composition (Fe/Sr = 3) had to be used. When the treatment was performed below 170 °C, ultrafine nanoparticles were formed. The TEM images show they have a disc-like shape, approximately 12 nm wide, but only around 4 nm thick. The EDS analysis showed their composition corresponded to $SrFe_{12}O_{19}$. When the temperature of the hydrothermal treatment exceeded 170 °C, larger hexagonal platelet crystals appeared as a consequence of Ostwald ripening. The evolution of the size and morphology of the nanoparticles with the temperature of the hydrothermal treatment was also monitored by XRD and measurement of the magnetic properties.

Introduction

Hexaferrites ($MFe_{12}O_{19}$, M = Ba, Sr) are industrially important magnetic materials that have numerous technological applications, for example, in permanent magnets, microwave devices, magnetic recording media and magneto-optical devices.[1,2]

Their suitability for these applications comes from a unique combination of magnetic and other properties, that is, a large magnetocrystalline anisotropy, a high Curie temperature, a large saturation magnetization and coercive field as well as good chemical stability and low cost.[3] Moreover, their magnetic properties can be tailored to the needs of a specific application, either by chemical substitution[4] or by controlling the size and shape of the crystals.[5,6] In particular, when the size of crystals is reduced to the nanoscale, the properties change dramatically. For example, the magnetic properties of ultrafine magnetic nanoparticles are dominated by the transition to the super-paramagnetic state. Super-paramagnetism occurs in ferri/ferromagnetic particles when their size is reduced below a certain critical size and thermal excitation induces rapid fluctuations in the particle's magnetic moment relative to the time of the observation.[7,8] Thus, super-paramagnetic nanoparticles, unlike larger ferro/ferrimagnetic particles, can be prepared in the form of stable suspensions as they show no agglomeration due to magnetic dipole–dipole interactions.[9]

[a] Department for Materials Synthesis, Jožef Stefan Institute, Jamova 39, 1000 Ljubljana, Slovenia
Fax: +386-1-4773-875
E-mail: darinka.primc@ijs.si
[b] Faculty for Chemistry and Chemical Engineering, University of Maribor,
Smetanova 17, 2000 Maribor, Slovenia

Stable colloidal suspensions of super-paramagnetic nanoparticles, so-called ferrofluids, are important for different technological applications,[9] including biotechnology and medicine, for example, in magnetic separation, as contrast-enhancement media in magnetic resonance imaging, as active constituents of drug-delivery platforms or as mediators for magnetic hyperthermia.[10]

Today, in practice, only the spinel-ferrite iron oxides magnetite and maghemite are used for biomedical applications, because they are considered non-toxic. However, due to their different, adjustable magnetic properties, hexaferrites could also be of great interest for use in biomedical applications. Pollert and co-workers[11] reported a negative cytotoxicity test for Sr hexaferrite nanoparticles, which suggests that they are a potential material for use in medical applications.

To prepare Sr hexaferrites in the form of a stable suspension, it is beneficial for the nanoparticles to be ultrafine, that is, to have a size close to the critical size for transformation to the super-paramagnetic state. This critical size depends on the magnetocrystalline anisotropy of the magnetic material and, due to a relatively high magnetocrystalline anisotropy, the critical size for hexaferrites is relatively small.[9] Theoretically, the critical size for hexaferrite nanoparticles is estimated to be a volume of approximately 300 nm^3, much smaller than that for soft-magnetic materials such as magnetite, for which it exceeds 4000 nm^3 (a diameter of ca. 20 nm for spherical particles).[9]

The synthesis of ultrafine nanoparticles of hexaferrite appears to be very difficult. This is because the formation temperature of hexaferrites is generally relatively high, typically above 600 °C, resulting in the formation of relatively large

particles.[11,12] Traditionally, Sr hexaferrite is prepared by solid-state synthesis; a stoichiometric mixture of raw materials (usually $SrCO_3$ and Fe_2O_3) is calcinated at high temperature, usually around 1100 °C.[11,12] The poor homogeneity of the mixture and the high temperatures usually result in the formation of relatively large, agglomerated particles with an uncontrolled particle morphology. Furthermore, calcination of a stoichiometric mixture (Fe/Sr = 12) usually results in the formation of a product containing hematite as the secondary phase.[12] Several wet methods, including co-precipitation,[13,14] sol–gel,[15,16] microemulsion,[17,18] sonochemical[19] and glass crystallization,[20,21] have also been employed to prepare a homogeneous Sr- and Fe-containing precursor, which was then subsequently calcinated to give hexaferrite particles at lower temperatures. However, even when the calcination temperature was as low as 600 °C,[11] the sizes of the particles remained above 50 nm. Alternatively, it has been shown in the case of Ba hexaferrite that nanoparticles can be obtained at moderate temperatures by using an in situ hydrothermal method without any subsequent high-temperature treatment.[22] During the hydrothermal synthesis, an aqueous suspension of precursor particles containing constituent ions, usually a mixture of the corresponding hydroxides, is treated in a sealed reactor at an elevated temperature and pressure, usually the equilibrium water pressure. The method is relatively simple and therefore appropriate for large-scale production. By using the hydrothermal method, Drofenik et al.[23] synthesized ultrafine, even super-paramagnetic, nanoparticles of Ba hexaferrite by dramatically reducing the formation temperature of the hexaferrite. This formation temperature was reduced by strongly increasing the concentration of hydroxide (OH^-) ions relative to the metal ions (Ba^{2+} and Fe^{3+}). Iron hydroxide is amphoteric and in an alkaline medium forms tetrahydroxidoferrate(III) $[Fe(OH)_4]^-$, which, under an increased concentration of hydroxide ions, presumably associate into iron-rich aggregates $[Fe(OH)_4]_n^{n-}$. These aggregates (optimally containing 12 units) combine much more easily with one Ba^{2+}, and consequently the supersaturation of hexaferrite and thus its nucleation is achieved at lower temperatures. The formation temperature of Ba hexaferrite can even be reduced to below 100 °C.[23]

For Ba hexaferrites, besides the formation temperature, also the mechanism by which the nanoparticles grow has a large influence on the size and the morphology of the synthesized nanoparticles. The nanoparticles formed at low temperatures by nucleation and limited primary growth had a uniform, disc-like shape, approximately 10 nm wide, but only approximately 3 nm thick. When the temperature of the hydrothermal treatment was increased, individual, large platelet crystals of Ba hexaferrite appeared as a consequence of secondary recrystallization (Ostwald ripening).[24]

Although there are many reports in the literature concerning the hydrothermal synthesis of Ba hexaferrite, the synthesis of Sr hexaferrite has been much less studied. Usually, the synthesis includes a calcination step following the hydrothermal treatment.[25,26]

However, it has also been shown that in situ hydrothermal synthesis can yield Sr hexaferrite particles without any subsequent heat treatment.[27,28] Recently, Jean et al.[28] showed that Sr hexaferrites can be synthesized by hydrothermal treatment of the precipitated strontium and iron hydroxides. Their work emphasizes the fact that Sr hexaferrite can be synthesized as μm-sized platelet crystals at a temperature of 180 °C. However, the synthesized products also contained the impurity phases, hematite and Sr carbonate.[27,28]

Although Sr carbonate can easily be dissolved in dilute mineral acids without affecting the Sr hexaferrite, the separation of hematite from the product is difficult. Because the presence of hematite causes a significant deterioration of the magnetic properties of the product,[27,28] the synthesis of the Sr hexaferrite without any hematite is important and still remains a challenge.

In this paper we report on the hydrothermal synthesis of ultrafine Sr hexaferrite nanoparticles. In the first part, the reasons for the parallel formation of unwanted hematite and the reaction conditions leading to hematite-free products are presented and discussed. The second part details the reaction conditions leading to the synthesis of ultrafine nanoparticles of Sr hexaferrite and their properties.

Results and Discussion

In the first part of this work, the origins of the unwanted parallel formation of hematite during the hydrothermal synthesis of Sr hexaferrite were studied. The metal hydroxides were precipitated from an aqueous solution using concentrated NaOH with various molar ratios of the metal ions (Fe^{3+}/Sr^{2+}), which was followed by hydrothermal treatment. Figure 1 shows the X-ray diffraction (XRD) patterns of the products hydrothermally synthesized by heating the autoclave to 200 °C. For the synthesis, different excesses of Sr ions in the system were used, whereas the OH^-/NO_3^- ratio was kept constant at 16. The XRD pattern of the sample 8M16, prepared with the smallest excess of Sr (Fe^{3+}/Sr^{2+} = 8) shows, besides Sr hexaferrite, also the presence of Sr carbonate and hematite. Quantification of the XRD pattern showed that the content of Sr carbonate is much lower than that predicted by the mass balance. The reason for this is the partial solubility of Sr carbonate in water;[29] Some of the Sr carbonate dissolved when the sample was washed after the synthesis. During the determination of the compositions of the samples, all three phases present were considered; however, only the contents of hexaferrite and hematite are listed in Table 1, normalized to 100 wt.-%. The content of hematite in the products decreased with increasing Sr excess. Apart from Sr carbonate and hexaferrite, the 8M16 sample contained 13 wt.-% hematite and the 5M16 sample (Fe^{3+}/Sr^{2+} = 5) only 5 wt.-% hematite. Finally, when the Fe^{3+}/Sr^{2+} molar ratio was set to 3, the sample 3M16 contained only Sr hexaferrite and Sr carbonate (Table 1).

Table 1. Phase compositions of the products hydrothermally synthesized at 200 °C using different starting compositions.[a]

Code	$n(Fe^{3+})/n(Sr^{2+})$[b]	$[OH^-]/[NO_3^-]$[c]	Hematite [wt.-%]	Sr hexaferrite [wt.-%]
12M16	12	16	100	0
8M16	8	16	13	87
5M16	5	16	5	95
5M16-Ar[d]	5	16	8	92
3M16	3	16	0	100

[a] Contents of hematite and Sr hexaferrite determined by XRD are normalized to 100%. Also, Sr-rich phases ($SrCO_3$) were considered in the analysis, but are not listed, because they partially dissolved during the washing of the product. [b] Molar ratio between metal ions (Fe^{3+}/Sr^{2+}) in the starting composition. [c] Ratio between nitrate and hydroxide ions in the starting composition. [d] Hydroxides were precipitated under argon.

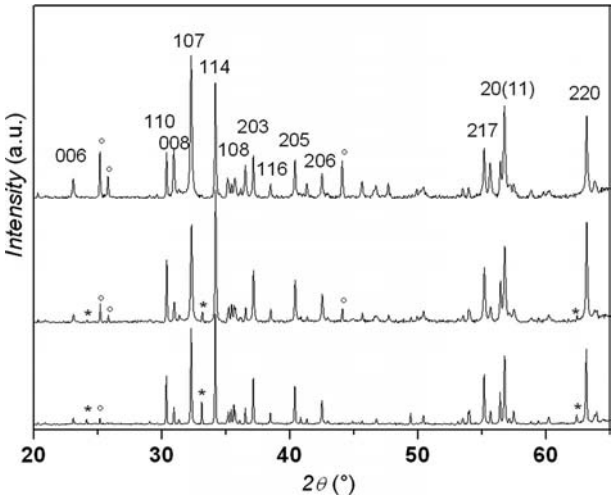

Figure 1. XRD patterns for samples 3M16 (top: Fe^{3+}/Sr^{2+} = 3), 5M16 (center: Fe^{3+}/Sr^{2+} = 5) and 8M16 (bottom: Fe^{3+}/Sr^{2+} = 8) show the influence of different Fe^{3+}/Sr^{2+} molar ratios in the starting composition on the phase composition after heating the autoclave to 200 °C. * denotes α-Fe_2O_3, and ° denotes $SrCO_3$.

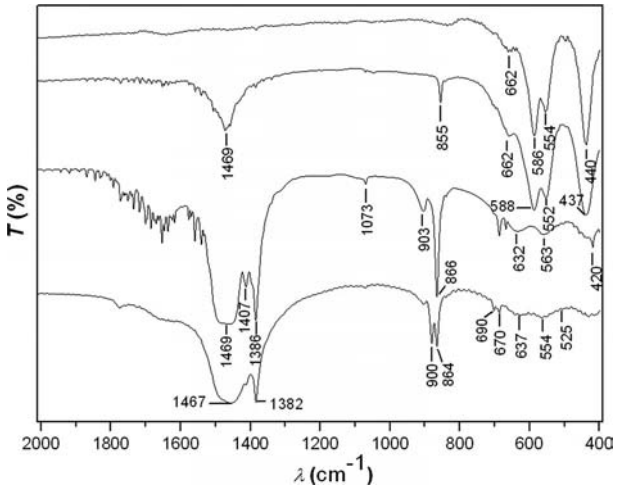

Figure 2. FTIR spectra of dried hydroxide precursors after precipitation at room temperature (3M16-20, second from the bottom) and after subsequent heating at 80 °C for 30 min. The heated samples differ in the starting composition; 3M16-80 (third from the bottom) was prepared with Fe^{3+}/Sr^{2+} = 3 and 8M16-80 (bottom) with Fe^{3+}/Sr^{2+} = 8. The FTIR spectrum of the sample M-200-0 (top) represents the spectrum of pure Sr hexaferrite.

To obtain further insights into the influence of excess Sr on the hexaferrite formation, the hydroxide precursors precipitated with different excesses of Sr ions were analysed. The precipitated precursors are poorly crystalline at temperatures below 100 °C and therefore XRD cannot be used for their analysis. Because their identification is, however, important for an understanding of phase evolution, an FTIR analysis was preformed (Figure 2). The precursors were separated from the suspension by centrifuge immediately after precipitation at room temperature or after subsequent heating at 80 °C for 30 min. To avoid later phase changes, the samples were dried in a vacuum at 40 °C. For comparison, a spectrum of pure Sr hexaferrite (M-200-0) is also shown.

The FTIR spectra of the dried precursors precipitated at room temperature (3M16-20) show narrow bands at 855, 1470, 1407 and 1470 cm^{-1}, which can be attributed to $SrCO_3$ and $Na_2CO_3 \cdot H_2O$, whereas the broad bands at 670, 690, 866 and 900 cm^{-1} correspond to precipitated iron species.[28,30,31] When the suspension of precursors with the largest amount of excess Sr was heated at 80 °C (3M16-80), the FTIR spectrum revealed the presence of narrow bands at 440, 552, 588 and 662 cm^{-1}, which indicates the partial formation of Sr hexaferrite, whereas the bands at 855 and 1469 cm^{-1} correspond to Sr carbonate.[30] In contrast, the FTIR spectrum of the heated precursor with the smallest amount of excess Sr (8M16-80) revealed no hexaferrite bands; however, a small band at 525 cm^{-1} is visible, which can be attributed to hematite.[31]

The results show that a large excess of Sr has to be available in the system to avoid the unwanted parallel formation of hematite. In general, the influence of excess Sr on the formation of the hematite can be ascribed to three factors.

(1) First, the need for Sr excess can be ascribed to the partial solubility of the precipitated Sr hydroxide, even at high pH. For example, the partial solubility of the precursor hydroxides was identified as the reason for the appearance of hematite in the case of the hydrothermal synthesis of $MnZnFe_2O_4$.[32] However, in the case of Sr hexaferrite, this is not likely to be the reason. Sr hydroxide is less soluble than Ba hydroxide.[29] If the solubility of Sr hydroxide could decisively influence the formation of hematite, the excess Sr needed to avoid the parallel formation of hematite would be less than the excess of Ba hydroxide in the case of the synthesis of Ba hexaferrite. However, Ba hexaferrite can be

obtained without the hematite secondary phase even with an Fe/Ba ratio of 8, which is less than that needed in the case of Sr hexaferrite.[33]

(2) Some of the Sr hydroxide reacts with CO_2 from the atmosphere to form Sr carbonate and is thus not involved in the formation of Sr hexaferrite, as proposed by other authors.[25,28] To evaluate the influence of atmospheric CO_2, the hydroxide precursors were precipitated in a CO_2-free environment under a continuous flow of argon to avoid a reaction between the Sr hydroxide and the CO_2. Quantification of the XRD pattern of the sample hydrothermally treated at 200 °C (5M16-Ar, Table 1) revealed that the absence of CO_2 had no significant influence on the phase composition. Apart from Sr hexaferrite and hematite, the sample 5M16-Ar also contained Sr carbonate, which formed after the reaction when the reaction vessel was opened and exposed to CO_2 in the ambient air.

(3) As a final possibility, kinetic reasons were considered. According to molecular collision theory, a larger excess of Sr increases the probability of successful collisions between the Sr species and the $[Fe(OH)_4^-]_x^{x-}$ complexes formed at high pH.[23] This assumption is in agreement with the results obtained from the FTIR analysis of the precursors. With the largest excess of Sr, the hexaferrite was detected even after heating the precursors at 80 °C. However, the FTIR spectrum suggested the formation of hematite instead of hexaferrite during the heating of the precursors with the smallest Sr excess at the same temperature. The formation of hematite under the applied conditions is in accordance with the literature report in which only iron hydroxide is hydrothermally treated.[31]

Clearly, a higher concentration of Sr ions shifts the formation of hexaferrite to lower temperatures for kinetic reasons. Because all the iron species in the sample with the largest excess of Sr were consumed for hexaferrite formation, the formation of hematite was not detected. In the case of a smaller Sr excess, the hexaferrite formation temperature is above the hematite formation temperature. When formed, hematite is stable and does not react further with Sr.

Once the experimental conditions required for the synthesis of Sr hexaferrite without the formation of hematite at the relatively high temperature of 200 °C had been determined, the influence of reaction temperature and time on the size and morphology of the particles was studied.

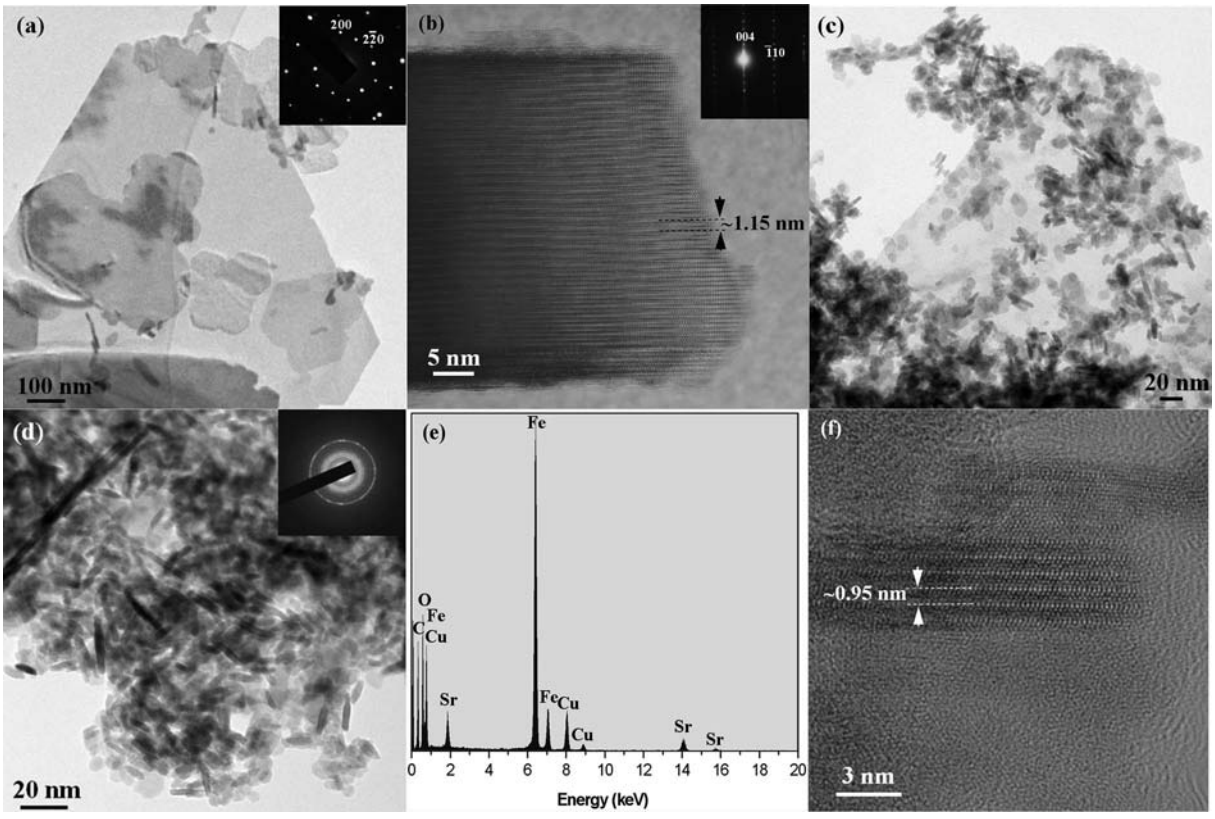

Figure 3. Sr hexaferrite nanoparticles M-200-0, M-180-0 and M-150-0, synthesized by heating the autoclave to various temperatures. (a) TEM micrograph of the sample synthesized at 200 °C. The corresponding electron diffraction pattern recorded from the largest platelet (inset of Figure 3a) is indexed according to the hexaferrite structure along the [001] direction. (b) HREM micrograph of the platelet crystal in the sample synthesized at 200 °C oriented with its large surfaces parallel to the electron beam. The largest periodicity of fringes corresponds to the (002) planes of the hexaferrite structure. Inset: Corresponding electron diffraction pattern. (c) TEM micrograph of the sample synthesized at 180 °C. (d) TEM micrograph of the sample synthesized at 150 °C. Inset: Corresponding electron diffraction pattern. (e) EDS spectrum of the ultrafine nanoparticles of the sample synthesized at 150 °C. Cu originates from the copper grid specimen support. (f) HREM image of the ultrafine disc-like nanoparticle oriented edge-on.

Figure 3a presents the transmission electron microscopy (TEM) micrograph of the sample M-200-0 synthesized by heating the autoclave to 200 °C. The sample is composed of large agglomerated crystals in the shape of hexagonal platelets. The crystals are approximately 200 to over 1000 nm wide, but only 20–40 nm thick. The electron diffraction pattern of the platelet crystal lying flat on the specimen support (inset of Figure 3a) corresponds to a hexaferrite structure in the [001] zone, which proves that the basal planes of the hexagonal hexaferrite structure are parallel to the large faces of the platelet crystals. Figure 3b is a high-resolution electron microscopy (HREM) image of the platelet crystal oriented edge-on with the large faces parallel to the electron beam. The periodicity of the fringes across the nanoparticle thickness of ca. 1.1 nm corresponds to the (002) planes of the Sr hexaferrite structure. The crystals show very good crystalline order and no amorphous surface layer.

When the temperature was decreased to 180 °C, the size and morphology of the synthesized products changed. Figure 3c, which is a TEM micrograph of the sample M-180-0, shows the presence of two types of particles. The majority of the sample was in the form of large platelet crystals. However, ultrafine nanoparticles with a uniform size are also visible. The ultrafine nanoparticles are agglomerated and stack on the larger crystals.

On reducing the reaction temperature the content of the ultrafine nanoparticles increased, whereas the content of the large platelet crystals decreased. Finally, when the temperature was reduced to below 170 °C, the samples contained only the ultrafine nanoparticles (Figure 3d).

The reaction time also influenced the morphology of the synthesized products. For example, when the time of the reaction at 160 °C was prolonged to 2 hours (M-160-2), large platelet crystals started to appear, whereas the majority of the sample was in the form of ultrafine nanoparticles. When the reaction time was further increased to 12 h (M-160-12), the product consisted of only the large platelet crystals (Table 2).

Figure 3e shows the energy-dispersive X-ray spectrum (EDXS) of an ultrafine nanoparticle. The nanoparticles contain Fe, Sr and O. Quantitative EDXS analysis of a large number of nanoparticles showed a composition corresponding to $SrFe_{12}O_{19}$, within the range of experimental uncertainty, which proves that they can be considered as Sr ferrite.

A detailed HREM analysis revealed that these ultrafine nanoparticles actually have a disk-like shape with an average diameter of around 12 nm and a thickness of approximately 4 nm. Figure 3f shows the HREM image of a disc-like nanoparticle oriented with its large faces parallel to the electron beam. The periodicity of the HREM pattern across the nanoparticle thickness was determined to be approximately 0.95 nm, significantly smaller than that in the larger crystals. In the HREM of the M hexaferrite crystal, the dominant periodicity along the *c* axis corresponds to the (002) plane.[22] According to data for the Sr hexaferrite structure (JCPDS No. 33-1340), the interplanar distance of (002) is equal to 1.15 nm, which was also measured in the HREM image of the larger Sr hexaferrite crystal (Figure 3b). The smaller periodicity experimentally observed across the thickness of the ultrafine nanoparticles can be related to the distortions in their structure due to their small size.

The electron diffraction pattern recorded for the ultrafine nanoparticles (inset of Figure 3d) corresponds to the hexaferrite structure. However, it provides little additional information on their structure, mainly because of the combination of their relatively complex structure (the cell parameters of the $SrFe_{12}O_{19}$ hexagonal structure are $a = 0.588$ nm and $c = 2.304$ nm) and their small size, especially their thinness (approximately 4 nm), which is of the order of only a few repetitions of the cell parameter along the *c* axis.

Table 2. Size, morphology and magnetic properties of the samples synthesized by hydrothermal synthesis under different reaction conditions.

Code	$n(Fe^{3+})/n(Sr^{2+})$[a]	$[OH^-]/[NO_3^-]$[b]	T [°C]	t [h]	Size [nm][c]	Morphology[d]	M_s[e] [A m²/kg]	H_c [$10^{-3}/(4\pi)$ A m^{-1}]
M-130-0	3	16	130	0	12.0 ± 2.1	ultrafine nanoparticles	0.40	133.4
M-150-0	3	16	150	0	12.0 ± 1.7	ultrafine nanoparticles	0.51	472.7
M-160-0	3	16	160	0	12.8 ± 1.9	ultrafine nanoparticles	0.63	466.1
M-160-2	3	16	160	2	12.8 ± 2.3[f]	ultrafine nanoparticles + platelet crystals	1.21	1059.7
M-160-12	3	16	160	12	–	platelet crystals	14.0	914.3
M-170-0	3	16	170	0	12.0 ± 1.8[f]	ultrafine nanoparticles + platelet crystals	3.06	1116.2
M-180-0	3	16	180	0	12.0 ± 3.0[f]	ultrafine nanoparticles + platelet crystals	8.72	1170.1
M-190-0	3	16	190	0	12.1 ± 1.7[f]	ultrafine nanoparticles + platelet crystals	28.67	1229.8
M-200-0	3	16	200	0	–	platelet crystals	40.8	1274.6

[a] Molar ratio of the metal ions (Fe^{3+}/Sr^{2+}) in the starting composition. [b] Ratio between nitrate and hydroxide ions in the starting composition. [c] The size was determined from a TEM micrograph, and it corresponds to the equivalent diameter of only the ultrafine disk-like Sr hexaferrite nanoparticles; the thickness was approximately 4 nm. [d] Morphology of the synthesized nanoparticles observed by TEM. The size of the platelet Sr hexaferrite crystals range from 200 to 1000 nm. [e] Specific magnetization measured at 1 T. [f] Samples contained Sr hexaferrite nanoparticles as ultrafine nanoparticles and large platelet crystals. However, to determine the particle size, only the ultrafine particles were considered.

As with the electron diffraction pattern, XRD also provides very limited information about the structure of the ultrafine nanoparticles. Figure 4 shows XRD spectra for the samples synthesized by heating the autoclave to different temperatures. The samples were washed with dilute acid to dissolve any Sr carbonate present as a consequence of the excess Sr in the starting composition. The XRD pattern of the sample synthesized at 200 °C (M-200-0) containing only the large platelet crystals shows only sharp reflections related to Sr hexaferrite (Powder Diffraction File Card No. 33-1340). The XRD patterns of the samples synthesized at lower temperatures, which predominantly contain the ultrafine nanoparticles, showed much lower intensities compared with the 200 °C sample. The positions of the reflections correspond to the hexaferrite structure. However, the relative intensities and the shapes of the peaks are very different to those of the "bulk". Finally, XRD patterns of the samples prepared at 150 and 130 °C, which only contained ultrafine nanoparticles, look very different to the pattern of the bulk. As we explained in the case of the ultrafine Ba hexaferrite nanoparticles,[23,24] the (*hkl*) reflections are missing for low *l* values due to the thinness of the crystallites along the *c* axis of their hexagonal hexaferrite structure. The diffraction patterns are additionally influenced by the preferential orientation that results from the platelet shape of the particles.

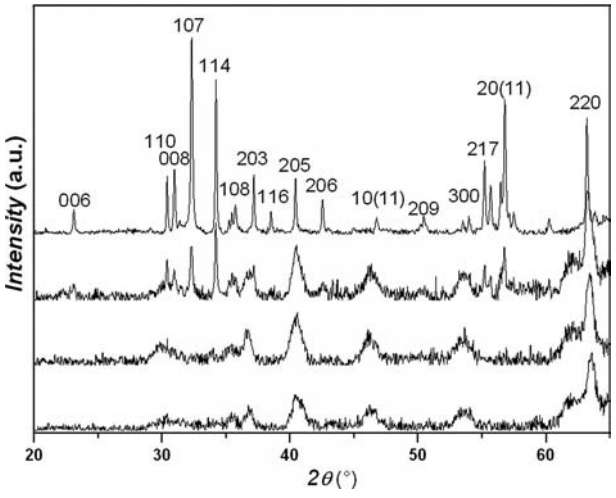

Figure 4. The XRD patterns for the samples synthesized by heating the autoclave to various temperatures; from the bottom up: 130 °C, 150 °C, 180 °C, 200 °C. The samples were washed with diluted acid to dissolve any Sr carbonate present as a consequence of the Sr excess in the starting composition. The intensities of the reflections were normalized to fit into one figure In reality, the intensities of the reflections recorded in the samples processed below 200 °C are much lower than those of the sample synthesized at 200 °C.

By systematically lowering the reaction temperature, it was found that the lowest temperature that led to the formation of the Sr hexaferrite nanoparticles was 130 °C. The average widths of the ultrafine disk-like particles, determined from the TEM micrographs of samples hydrothermally treated at different temperatures, are listed in Table 2. The size remained almost constant in the temperature range 130–190 °C. This suggests that the primary growth after nucleation of the particles is very limited. Most probably, the majority of the reactants are consumed during the formation of nuclei, leaving almost no material available for growth. At approximately 170 °C, the secondary recrystallization (Ostwald ripening) starts, resulting in the appearance of larger platelet crystals. In this process, individual small nanoparticles grow, whereas other nanoparticles dissolve. Finally, all the ultrafine nanoparticles were consumed by the secondary recrystallization at temperatures above 190 °C.

The magnetic measurements revealed the influence of the size and shape of particles on the magnetic properties of the synthesized nanoparticles (Table 2). For the magnetic measurements, the nanoparticles were washed with dilute nitric acid to dissolve any excess Sr-rich particles present as a consequence of the excess Sr. Figure 5a shows the magnetic hysteresis loops for the Sr hexaferrite particles synthesized at different temperatures. For the sample synthesized at 200 °C (M-200-0), the saturation magnetization (M_s, measured at 1 T) is equal to 40.8 $A m^2/kg$, which is much smaller than the bulk magnetization (74.3 $A m^2/kg$). Also, the measured coercive field ($1275 \times 10^3/(4\pi)$ $A m^{-1}$) is relatively low. Typically, $SrFe_{12}O_{19}$ nanoparticles prepared by other soft chemical methods exhibit coercivities of 4000 Oe and more.[11] The low coercivities of the synthesized platelet crystals indicate soft magnetic behaviour, which is a consequence of the large shape anisotropy (the platelet crystals are highly anisotropic) and the nucleation of domain walls, also known as the Brownian paradox.[34,35] With decreasing temperature the saturation magnetization decreased. For the sample synthesized at 190 °C, the saturation magnetization is equal to 28.7 $A m^2/kg$, whereas for the sample synthesized at 180 °C, it is only 8.7 $A m^2/kg$. The strong decrease in M_s can be attributed to an increased portion of ultrafine Sr hexaferrite nanoparticles in the synthesized products.

Coercivities for the samples M-190 and M-180, dominated by the large platelet crystals, remain approximately the same as in the sample M-200-0 treated at higher temperature. The small changes in the coercivities indicate that with an increased synthesis temperature the proportion of the large platelets increases rather than their size.

Figure 5b shows the magnetic hysteresis loops for the samples consisting of only ultrafine Sr hexaferrite nanoparticles. The magnetizations (measured at 1 T) for the samples M-160, M-150 and M-130 were rather low, below 1 $A m^2/kg$ (Table 2), whereas the coercivities were around $470 \times 10^3/(4\pi)$ $A m^{-1}$ for the samples M-150 and M-160, and $130 \times 10^3/(4\pi)$ $A m^{-1}$ for M-130. These low coercivities suggest that the majority of the particles are in, or close to, the super-paramagnetic state. In part, the very large decrease in the magnetizations of the ultrafine nanoparticles can be ascribed to their large surface-to-volume ratio and consequently the increased proportion of surface atoms. These surface atoms have an incomplete coordination, which leads to a non-collinear spin configuration,[23,35] resulting in a reduction of the saturation magnetization. However, the main

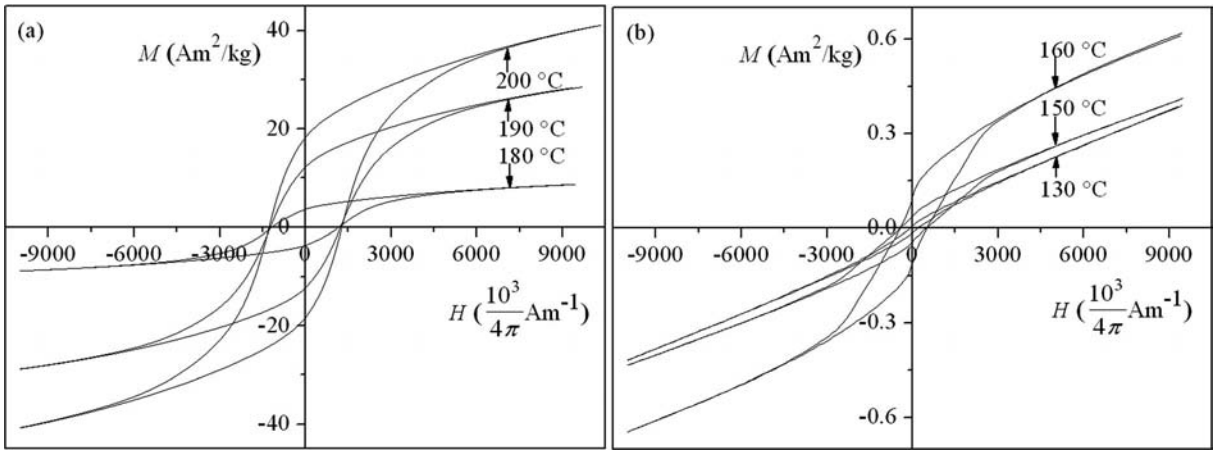

Figure 5. Magnetic hysteresis for the Sr hexaferrite nanoparticles synthesized at different reaction temperatures. The samples synthesized in the temperature range 180–200 °C were composed of large platelet crystals and ultrafine nanoparticles (a), whereas the samples synthesized between 130 and 160 °C consisted of only the ultrafine Sr hexaferrite nanoparticles (b).

reason for the low magnetizations is most probably related to changes in the magnetic order of the nanoparticles due to their very small size, especially their thinness, which is of the order of their cell parameter in the *c* axis of the structure. Müller and co-workers[36,37] synthesized Ba hexaferrite nanoparticles using a glass crystallization method. The nanoparticles were comparable in size to the broadness of the disc-like nanoparticles. However, the disc-like nanoparticles have one dimension, which is still much smaller, their thickness corresponding to the *c* axis of the structure, which decisively defines the structural and magnetic properties of the hexaferrite.

Conclusions

Ultrafine strontium hexaferrite ($SrFe_{12}O_{19}$) nanoparticles have been synthesized by the hydrothermal treatment of an appropriate suspension of Sr and Fe hydroxides at temperatures between 130 and 170 °C. A large excess of Sr in the starting composition (Fe/Sr = 3) was needed to avoid the parallel formation of unwanted hematite. The excess Sr lowers the formation temperature of the hexaferrite for kinetic reasons to temperatures lower than that required for hematite formation. The hexaferrite formed at temperatures below 170 °C was in the form of ultrafine nanoparticles with a disk-like shape, approximately 12 nm wide and 4 nm thick. At higher temperatures, the hydrothermal treatment led to larger platelet crystals as a result of Ostwald ripening. The ultrafine Sr hexaferrite nanoparticles showed weak magnetic properties with a magnetization below 1 Am^2/kg (measured at 1 T).

Experimental Section

Materials: Iron(III) nitrate [$Fe(NO_3)_3{\cdot}9H_2O$], strontium nitrate [$Sr(NO_3)_2$] and sodium hydroxide (NaOH), were purchased from Alfa Aesar. The exact iron content in the $Fe(NO_3)_3{\cdot}9H_2O$ was determined by using inductively coupled plasma mass spectrometry (ICP-AES, Thermo Jarrell Ash, model Atomscan 25).

Synthesis of the Nanoparticles: Strontium hexaferrite nanoparticles were hydrothermally synthesized in a 1000 mL Inconel autoclave vessel (model 4522 M, Parr Instrument Co.) without any agitation. First, the exact amounts of iron and strontium nitrates were dissolved in distilled water (400 mL). The amount of iron(III) nitrate was kept constant at 20.8 mmol, whereas the amount of strontium nitrate was varied (2.6 mmol, 4.16 mmol, and 6.6 mmol) to give Fe^{3+}/Sr^{2+} molar ratios of 8, 5 and 3. Secondly, sodium hydroxide was dissolved in the solution of metal ions to give an $[OH^-]/[NO_3^-]$ ratio of 16. The addition of NaOH resulted in the precipitation of hydroxide precursors. The suspension of precursors was then sealed in the autoclave vessel and heated at a heating rate of 3 °C/min to various temperatures ranging from 130 to 200 °C. The autoclave was maintained at the final temperature for different times (0–12 h) before the heat was turned off. The temperature was measured by using a probe inside the autoclave. Because of the relatively large thermal capacity, the temperature remained at the listed value ±2 K for approximately 10 min even when the time was set to 0. After the synthesis, each product was thoroughly washed with distilled water and dried at 60 °C in ambient air. Table 1 lists the starting compositions for the different samples, and Table 2 lists the experimental conditions used for their hydrothermal synthesis. In the majority of experiments, a mixture of hexaferrite and Sr carbonate was obtained as a consequence of the excess Sr in the starting composition. To obtain pure Sr hexaferrite nanoparticles, the samples were thoroughly washed with dilute nitric acid (5 wt.-%). Nitric acid easily dissolves any Sr-rich compounds, whereas Sr hexaferrite is completely insoluble. Finally, the particles were washed with distilled water and then dried at 60 °C in ambient air.

Characterization: The synthesized particles were characterized by X-ray diffraction (XRD, PANalytical X' Pert PRO) and transmission electron microscopy (TEM). The phase compositions of the powders were quantified from refinements of the XRD spectra using the Rietveld method[38] with the crystallographic program Topas2R 2000 from Bruker AXS. The estimated relative total error of the analysis was ±10%. For the TEM investigations, the nanoparticles were deposited on a perforated transparent carbon foil supported on a copper grid. A field-emission electron-source transmission electron microscope (JEOL 2010 F) equipped with an energy-dispersive X-ray spectrometer (EDXS, LINK ISIS EDS 300) was operated at 200 kV. Quantitative EDX analyses were performed by using Oxford ISIS software. The spectrum of the large, well-crystallized platelet crystals of $SrFe_{12}O_{19}$ of the sample M-

200-0 was used as a standard during the quantization of the spectra collected from the ultrafine nanoparticles. The relative standard deviation of the measurements from 10 spectra acquired from the same crystal was determined to be ±0.25% for Fe and ±0.3% for Sr. The magnetic properties of the materials were measured at room temperature using a vibrating-sample magnetometer (LakeShore VSM 7307).

Acknowledgments

The support of the Ministry of Higher Education, Science and Technology of the Republic of Slovenia within the National Research Program is gratefully acknowledged. The authors thank Dr. Saso Gyergyek for his help with the magnetic measurements. The authors also acknowledge the use of equipment at the Center of Excellence on Nanoscience and Nanotechnology – Nanocenter.

[1] P. Hernandez, C. D. Francisco, J. M. Munoz, J. Iniguez, L. Torres, M. Zazo, *J. Magn. Magn. Mater.* **1996**, *157–158*, 123–124.
[2] Z. Jin, W. Tang, J. Zhang, H. Lin, Y. Du, *J. Magn. Magn. Mater.* **1998**, *182*, 231–237.
[3] Y. Fu, K. Pan, *J. Alloys Compd.* **2003**, *349*, 228–231.
[4] N. J. Shirtcliffe, S. Thompson, E. S. O'Keefe, S. Appleton, C. C. Perry, *Mater. Res. Bull.* **2007**, *42*, 281–287.
[5] D. Makovec, M. Drofenik, *Cryst. Growth Des.* **2008**, *8*, 2182–2186.
[6] M. M. Heissen, M. M. Rashad, K. El-Barawy, *J. Magn. Magn. Mater.* **2008**, *320*, 336–343.
[7] X. Batlle, A. Labarta, *J. Phys. D: Appl. Phys.* **2002**, *35*, R15–R42.
[8] R. H. Kodama, *J. Magn. Magn. Mater.* **1999**, *200*, 359–372.
[9] S. Odenbach in *Ferrofluids, The Preparation of Magnetic Fluids* (Eds.: R. Beig, B. G. Englert), Springer, Berlin, Heidelberg, **2002**, pp. 3–18.
[10] Q. A. Pankhurst, J. Connolly, S. K. Jones, J. Dobson, *J. Phys. D: Appl. Phys.* **2003**, *36*, R167–R181.
[11] P. Veverka, K. Knížek, E. Pollert, J. Boháček, S. Vasseur, E. Duguet, J. Portier, *J. Magn. Magn. Mater.* **2007**, *309*, 106–112.
[12] H. R. Koohdar, S. A. Seyyed Ebrahimi, A. Yourdkhani, R. Dehghan, F. Zajkaniha, *J. Alloys Compd.* **2009**, *479*, 638–641.
[13] D. H. Chen, Y. Y. Chen, *Mater. Res. Bull.* **2002**, *37*, 801–810.
[14] S. E. Jacobo, C. Domingo-Pascual, R. Roudrigez-Clemente, M. Blesa, *J. Mater. Sci.* **1997**, *32*, 1025–1028.
[15] C. Sürig, K. A. Hempel, D. Bonnenberg, *Appl. Phys. Lett.* **1993**, *63*, 2836–2838.
[16] J. H. Choy, J. S. Han, S. W. Song, *Mater. Lett.* **1994**, *19*, 257–262.
[17] J. Fang, J. Wang, L. M. Gan, S. C. Ng, J. Ding, X. Liu, *J. Am. Ceram. Soc.* **2000**, *83*, 1049–1055.
[18] D. H. Chen, Y. Y. Chen, *J. Colloid Interface Sci.* **2001**, *236*, 41–46.
[19] K. V. P. M. Shafi, I. Felner, Y. Mastai, A. Gedanken, *J. Phys. Chem. B* **1999**, *103*, 3358–3360.
[20] H. Sato, T. Umeda, *Matter Trans.* **1993**, *34*, 76–81.
[21] B. T. Shirk, W. R. Buessem, *J. Am. Ceram. Soc.* **1970**, *53*, 192–196.
[22] M. Drofenik, M. Kristl, A. Žnidaršič, D. Hanžel, D. Lisjak, *J. Am. Ceram. Soc.* **2007**, *90*, 2057–2061.
[23] M. Drofenik, I. Ban, G. Ferk, D. Makovec, A. Žnidaršič, Z. Jagličič, D. Lisjak, *J. Am. Ceram. Soc.* **2010**, *93*, 1602–1607.
[24] D. Primc, D. Lisjak, D. Makovec, M. Drofenik, *Nanotechnology* **2009**, *20*, 315605.
[25] A. Ataie, I. R. Harris, C. B. Ponton, *J. Mater. Sci.* **1995**, *30*, 1429–000.
[26] J. F. Wang, C. B. Ponton, R. Grössinger, I. R. Harris, *J. Alloys Compd.* **2004**, *369*, 170–177.
[27] H. J. Lee, H. S. Kim, C. W. J. Won, *Mater. Sci. Lett.* **1996**, *15*, 295–297.
[28] M. Jean, V. Nachbaur, J. Bran, J. M. Le-Breton, *J. Alloys Compd.* **2010**, *496*, 306–312.
[29] N. N. Greenwood, A. Earnshaw, *Chemistry of the Elements*, Elsevier, Oxford, **2006**, p. 121.
[30] S. Kong, P. Zhamg, X. Wen, P. Pi, J. Chen, Z. Yang, J. Hai, *Particuology* **2008**, *6*, 185–190.
[31] R. M. Cornell, U. Schwertmann, *The Iron Oxides*, Wiley-VCH, Weinheim, **2003**, pp. 141–147.
[32] M. Rozman, M. Drofenik, *J. Am. Ceram. Soc.* **1995**, *78*, 2449–2455.
[33] Y. Liu, N. G. B. Drew, J. P. Wang, M. L. Zang, Y. Liu, *J. Magn. Magn. Mater.* **1999**, *195*, 452–459.
[34] B. D. Cullity, C. D. Graham in *Introduction to Magnetic Materials* (Ed.: L. Hanzo), IEEE Press, New Jersey, **2009**, pp. 374.
[35] J. E. Knowles, *IEEE Trans. Magn.* **1984**, *20*, 84–86.
[36] P. Görnet, H. Pfeiffer, E. Sinn, R. Müller, W. Schüppel, M. Rösler, X. Batlle, M. Garcia del Muro, J. Tejada, S. Gali, *IEEE Trans. Magn.* **1994**, *30*, 714–716.
[37] R. Müller, R. Hiergeist, H. Steinmetz, N. Ayoub, M. Fujisaki, W. Schüppel, *J. Magn. Magn. Mater.* **1999**, *201*, 34–37.
[38] H. M. Rietveld, *Acta Crystallogr.* **1967**, *22*, 151–152.

Received: March 28, 2011
Published Online: July 25, 2011

